

# On-Demand Polarization Controllable Liquid Crystal Laser

Taimoor Ali, Steve J. Elston, Jia-De Lin, and Stephen M. Morris\*

A polarization controllable band-edge liquid crystal (LC) laser configuration is presented that provides on-demand control of the polarization state of the laser using a four electrode in-plane configuration to drive a nematic LC layer. By controlling the orientation of the electric field, and thus the orientation of the optic axis of the nematic LC, as well as the retardance, any laser polarization state (e.g., circular, elliptical) can, in principle, be created that is aligned along any desired direction in a plane perpendicular to the propagation direction. After calibrating the tuneable nematic device with a He-Ne laser that has a well-defined polarization state, control of the LC laser polarization is then demonstrated, where it is shown that different polarization states and orientations thereof can be obtained by changing the relative combination and amplitudes of the voltages applied to each of the four electrodes. It is found, however, that achieving a pure linear polarization state is challenging, which may indicate that the polarization from the LC laser is not a well-defined circularly polarized state. These thin-film LC lasers with full polarization control are potentially important for a variety of different applications ranging from the biomedical to the display industries.

band-edge, the laser emission is considered to be circularly polarized, which can be either right or left-circularly polarized depending upon the handedness of the helix.

For many applications, including high-contrast LC displays,<sup>[20]</sup> optoelectronic devices,<sup>[21]</sup> optical communication systems,<sup>[22]</sup> optical measurements,<sup>[23]</sup> fiber optics,<sup>[24]</sup> polarimetric<sup>[25]</sup> and holographic imaging,<sup>[26]</sup> 3D displays,<sup>[27]</sup> and virtual reality (VR)/augmented reality (AR) displays,<sup>[28]</sup> manipulating the polarization state of light is of considerable importance. Toward this end, and to enable direct control of the polarization of a laser source, a range of different polarization controllers have been developed over the years. For example, polarization controllers have been created using silicon lab-on-chip photonic integrated circuits by forming waveguides and structures that can encode and process optical information.<sup>[29]</sup>

Such systems, however, typically require sophisticated fabrication processing that ultimately leads to an increase in the device cost as well as limitations in terms of tuneability. Liquid crystalline materials, on the other hand, are relatively easy to process and are compatible with cost-effective fabrication techniques. Furthermore, they exhibit electro-optic characteristics that enable them to be used as polarization rotators.<sup>[30–32]</sup> As an example, an early incarnation of an LC-based optical rotator was demonstrated by Ye<sup>[33]</sup> using two quarter waveplates. An optical modulator followed later by Davis et al. who demonstrated 2D polarization phase encoding in an LC spatial light modulator.<sup>[34]</sup>

It is well-known that when an electric field is applied across a nematic LC layer, the reorientation of the director can result in a change in the optical retardation ( $\Delta n \cdot d$ ), which enables the optical properties to be tuned to different waveplate conditions (e.g., quarter-wave plate, half-wave plate, etc.). As a result, depending on the strength of the electric field, circularly polarized light can be changed to elliptically or linearly polarized light. By making use of this electro-optic behavior, various device configurations have been presented that use nematic,<sup>[35]</sup> chiral nematic<sup>[36]</sup> or a combination of LC phases<sup>[37]</sup> to manipulate the polarization state of light.<sup>[38–42]</sup> Moreover, a polarization tuneable chiral nematic LC laser has been demonstrated previously<sup>[43]</sup> where the polarization state of the output can be controlled. However, in accordance with the findings reported for other polarization devices, the control of the polarization was limited as the orientation of the polarization state could not be controlled directly. In another configuration that has been reported,<sup>[44]</sup> the orientation of the polarization state of a

## 1. Introduction

Liquid crystal (LC) lasers<sup>[1,2]</sup> have received considerable attention over the past 20 years because of the advantageous features that they exhibit including low excitation threshold energies,<sup>[3–7]</sup> high slope efficiencies,<sup>[8]</sup> tuneability,<sup>[9–16]</sup> compatibility with conformable/flexible substrates<sup>[17,18]</sup> and the ability to be optically pumped using solid-state compact laser diode technology.<sup>[19]</sup> Of the various incarnations that have been demonstrated, chiral nematic (cholesteric) band-edge LC lasers have been the ones that have been most intensely studied. Due to the macroscopic helical structure and the nature of the resonant modes at the

T. Ali, S. J. Elston, S. M. Morris  
Department of Engineering Science  
University of Oxford  
Parks Road, Oxford OX1 3PJ, UK  
E-mail: stephen.morris@eng.ox.ac.uk

J.-D. Lin  
Department of Opto-Electronic Engineering  
National Dong Hwa University  
Hualien 974, Taiwan

The ORCID identification number(s) for the author(s) of this article can be found under <https://doi.org/10.1002/admt.202200674>.

© 2022 The Authors. Advanced Materials Technologies published by Wiley-VCH GmbH. This is an open access article under the terms of the Creative Commons Attribution License, which permits use, distribution and reproduction in any medium, provided the original work is properly cited.

DOI: 10.1002/admt.202200674

defect-mode laser created with two identical 1D photonic crystals comprising alternating  $\text{SiO}_2$ - $\text{TiO}_2$  layers was controlled with a nematic LC layer by applying an in-plane field. However, the number of alternating layers of  $\text{SiO}_2$ - $\text{TiO}_2$  was crucial in creating a well-defined polarization state. In addition, the fabrication process was rather complex as six in-plane electrodes were required, and the fabrication steps had to be repeated several times to create a 1D photonic crystal with a multilayered structure.

In this study we demonstrate both the control and tunability of the polarization state of a band-edge LC laser with an all-LC based device using a four electrode in-plane assembly. The in-plane electrode configuration ensures that the applied electric field provides control of the azimuthal orientation as well as the tilt of the LC director, allowing for both simultaneous control of the orientation and retardation of the LC waveplate. Using this configuration, it is then possible to control fully the polarization state of the LC laser output. Engineering both the ellipticity and orientation of the polarization state of the light emitted from these lasers could be of significant benefit for applications relating to holographic imaging tools and VR/AR displays.

## 2. The Polarization Controller

A planar-aligned nematic LC device can act as a tuneable waveplate when a transverse electric field is applied across the device. In this way, it is possible to vary the polarization state depending on the retardation introduced by the LC layer. The orientation of the polarized light, however, is arbitrary and depends on the orientation of the optical axis of the nematic LC.

The orientation can be changed if the planar-aligned nematic LC device is physically reoriented to a specific angle so that the polarization state aligns in a particular direction. Whilst functional, this approach suffers from the fact that it is necessary to mechanically reorient the device, which is not generally practical for most applications.

Instead, in order to electrically control both the polarization state (e.g., linear, circular, elliptical) as well as the orientation of the polarization state, here we propose the use of a nematic LC (E7, Synthon Chemicals Ltd.) that is homeotropically aligned and that is subjected to an in-plane (relative to the device substrates) electric field. This tuneable nematic LC layer is combined with an LC band-edge laser to demonstrate both the controllability of the polarization state and its orientation. To generate an electric field of any orientation in the plane, the device architecture consists of four identical electrodes that are subjected to different combinations of voltages and different amplitudes. The resulting device arrangement is presented schematically in **Figure 1** (see also Figure S1, Supporting Information) for an illustration of the change in the alignment of the LC director with the application of an electric field in the plane of the device). Here, the LC band-edge laser comprises a laser dye that is dispersed into a chiral nematic LC host. The gain material is chosen so that its peak fluorescence emission wavelength overlaps with the long-wavelength edge of the photonic bandgap. Laser emission is generated at the edge of the bandgap when optically pumped by a short pulse width solid state laser (e.g., the second harmonic of an Nd:YAG laser). The tuneable nematic LC device that follows the band-edge laser then controls and varies the polarization state of the laser emission. The exact nature and orientation of the

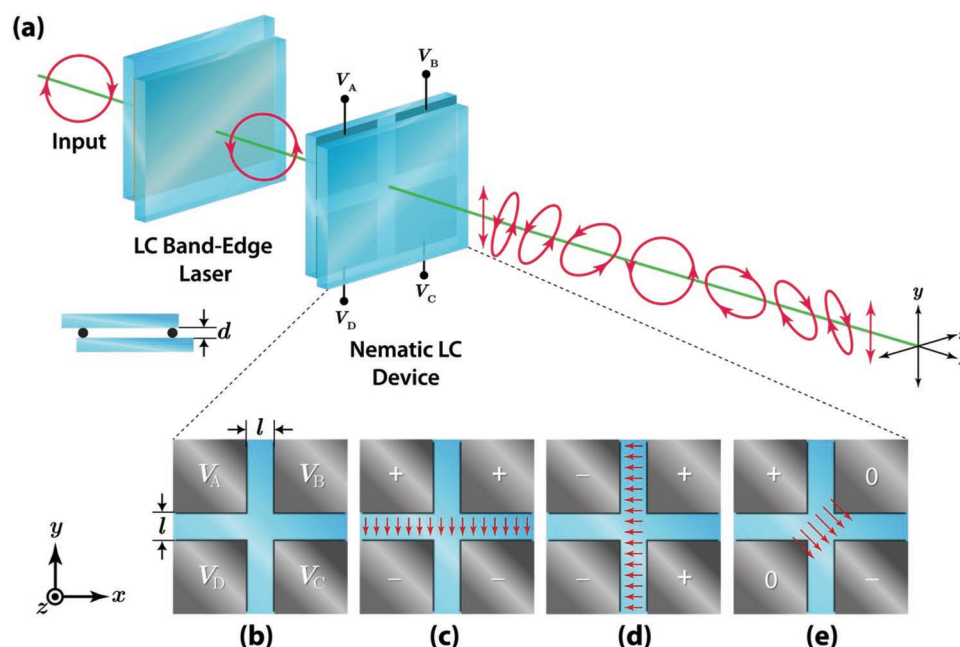


**Figure 1.** a) An illustration depicting the control of both the polarization state (e.g., linear, circular, elliptical) and the orientation of the polarization state of a band-edge LC laser using a nematic LC device (cell gap  $d$ ) with an in-plane electric field. b) The in-plane electrode assembly with four patterned electrodes with electrode spacing ( $l$ ). Each electrode is electrically isolated with voltages  $V_A$ ,  $V_B$ ,  $V_C$ , and  $V_D$ . Example images showing three situations for generating an electric field along the following directions relative to the  $-y$ -axis (where clockwise angles are taken as positive values): c)  $0^\circ$ , d)  $90^\circ$ , and e)  $-45^\circ$ , which are achieved by applying different combinations of voltages to the electrodes.

polarization state depends on the combination and orientation of the electric field generated by the four-electrode configuration (*vide infra*).

## 2.1. Controlling the Electric Field Orientation

The magnitude and polarity of the applied voltages on the electrodes are critical in terms of generating an electric field along a desired orientation. It is, therefore, important to estimate the applied voltages that needed to be applied to each of the electrodes. For this, let us consider the electrode assembly as shown in Figure 1b. For simplicity, we consider that the voltages at the corner of each electrode are  $V_A$ ,  $V_B$ ,  $V_C$ , and  $V_D$ , and that the electrode gap is " $l$ ". The desired electric field to be generated at the center region between the electrodes is thus  $E = E_x + E_y$ , where  $E_x$  and  $E_y$  are the electric fields along the  $x$  and  $y$  directions, respectively, and take the form

$$E_x = E_i \sin(\psi) \quad (1)$$

$$E_y = E_i \cos(\psi) \quad (2)$$

where  $\psi$  is the orientation with respect to the  $-y$ -direction of the desired electric field and  $E_i$  is the target electric field required. Using these expressions, the voltage at each electrode can then be approximated as

$$V_A = \frac{l}{2}(-E_x + E_y) \quad (3)$$

$$V_B = \frac{l}{2}(E_x + E_y) \quad (4)$$

$$V_C = \frac{l}{2}(E_x - E_y) \quad (5)$$

$$V_D = \frac{l}{2}(-E_x - E_y) \quad (6)$$

Using Equations (1)–(6), the voltage on each electrode can then be estimated to create an electric field along any desired orientation. In this regard, a COMSOL Multiphysics model for an equivalent in-plane electrode device was created with a material with an isotropic dielectric permittivity, and simulations were carried out to demonstrate the electric field along various orientations  $0^\circ$ ,  $+90^\circ$ ,  $+45^\circ$ ,  $-45^\circ$  (with respect to the  $-y$ -direction). The electrode separation was set to  $500 \mu\text{m}$  to match that of the experiments. Example simulation results are presented in Figure 2. It can be seen that the electric field along the vertical orientation (i.e., along  $0^\circ$ ) is generated for the condition as follows: 1)  $V_A = V_B$  and  $V_C = V_D$ ; 2)  $V_A$  and  $V_B$  are set to positive values; and 3)  $V_C$  and  $V_D$  are set to negative voltages, Figure 2a. Alternatively, for the  $+45^\circ$  case,  $V_A = V_C = 0 \text{ V}$ ,  $V_B = +V$ , and  $V_D = -V$ , Figure 2c. This implies that by correctly choosing a suitable combination of voltages and subsequent

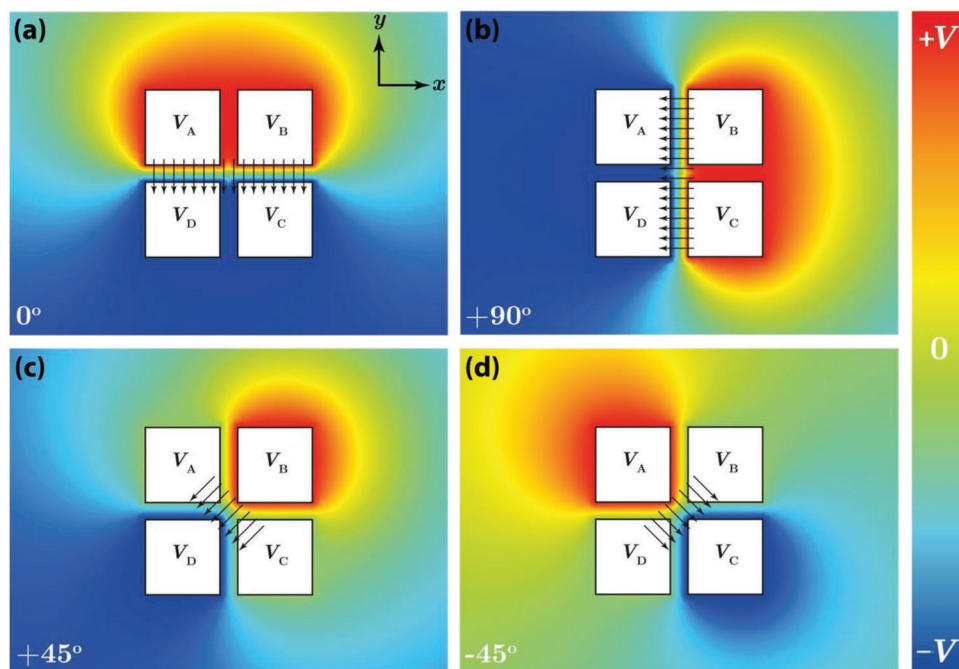


**Figure 2.** COMSOL Multiphysics model of the electric field profile for a homeotropically aligned nematic LC device (assuming an isotropic dielectric permittivity) with a four-electrode in-plane configuration when different voltage conditions are applied to the electrodes. The electrode spacing ( $l$ ) was set to  $500 \mu\text{m}$ . In this case, the electrodes are labeled as  $V_A$ ,  $V_B$ ,  $V_C$ , and  $V_D$  in the figure, and together these enable the generation of an electric field at any orientation in the plane of the device. In the figure, the following orientations of the electric field are demonstrated: a)  $0^\circ$ , b)  $+90^\circ$ , c)  $+45^\circ$ , and d)  $-45^\circ$  (all of which are with respect to the  $-y$ -direction). These results have been obtained when different combinations of voltages were applied to the electrodes.



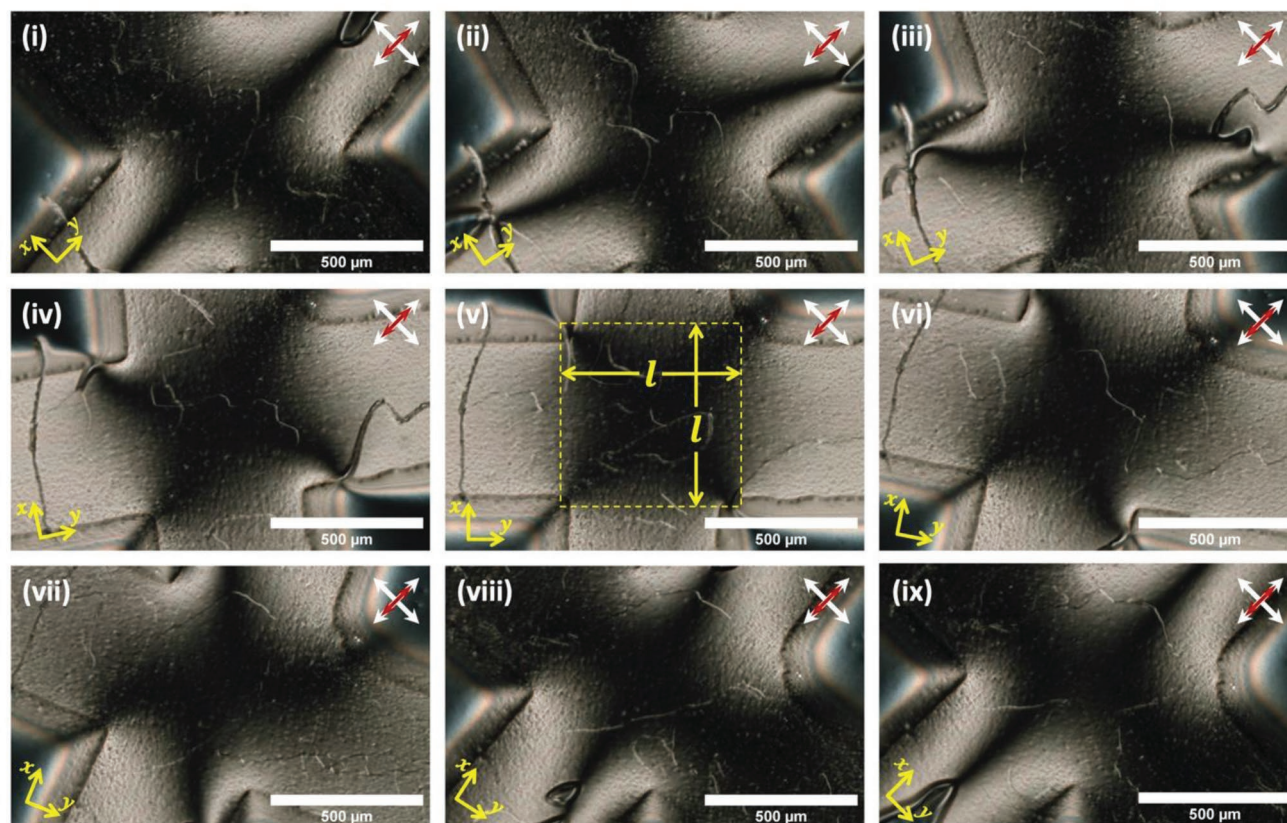


**Figure 3.** Polarized optical microscope images of the homeotropically aligned nematic LC device with the four-electrode in-plane configuration. Images are presented for different combinations of voltages that were applied to the four electrodes in order to align the electric field along different orientations with respect to the coordinates defined in Figure 1. The device was then rotated in the plane so that the electric field aligned with the axis of the polarizer. The orientation of the electric field is represented by the double-headed red arrow in the top right corner of each image while the white double-headed arrows in the crossed configuration represent the orientation of the polarizer and analyzer. The yellow single-headed arrows in the bottom left corner show the orientation of the device for the coordinate axes defined in Figure 1. The corresponding voltages applied to each electrode are given in Table 1. The scale bar in each image is 500  $\mu\text{m}$ .

relative amplitudes, an electric field can be generated that is preferentially along any desired orientation in the plane of the device.

The electro-optic switching behavior of the homeotropically aligned nematic LC (E7) device was investigated by generating an electric field along a certain orientation in the plane of the device (Figure 3). For this investigation, the device was observed between crossed polarizers on a polarized optical microscope and each electrode of the device was connected to a waveform generator (FLC WFG 500) that could generate a square wave of 100 kHz up to  $\pm 100$  V. The electrode separation was set to  $l = 500$   $\mu\text{m}$  (as illustrated in Figure 1) and the cell gap was chosen to be  $d = 50 \pm 2$   $\mu\text{m}$ . The cell gap was chosen based upon the inverse relationship between the electric field threshold for switching and the device thickness: for in-plane electrodes, larger cell gaps result in lower critical electric field thresholds. However, cell gaps that are too large can compromise the quality of the homeotropic alignment. Furthermore, in these thick devices with moderate amounts of distortion the surface torques are not strong and so the anchoring is assumed to be “strong”.

The electrode separation was chosen as it is substantially larger than the output beam size of the LC laser, was readily

accessible using conventional photolithography techniques, and ensured that the central region between the electrodes (through which the LC laser beam passes) was free from defects that might arise around the electrode edges. Larger apertures for the nematic LC device could be employed (spacings of the electrodes), but this will require larger drive voltages. An “ideal” electrode separation/aperture would perhaps be one that closely matches the output beam size of the LC laser, but at the same time minimizes the presence of defects in the central region of the aperture and does not require inordinately large driving voltages. The square wave voltages that were applied to the electrodes had the same phases. The frequency of the device was set to 100 kHz as it was observed that at this frequency the defects in the alignment generated in the nematic LC were minimized. Figure S2 of the Supporting Information shows example images of the optical texture when the device was subjected to low frequency ( $<1$  kHz) and high frequency ( $>1$  kHz) electric fields, where it can be seen that there is a greater concentration of defects at low frequencies. A four-channel digital storage oscilloscope (Tektronix TDS2004B, 60 MHz, 1 GS  $\text{s}^{-1}$ ) was also used to test the level of each signal from the waveform generator to confirm the peak amplitude of the applied voltage.

**Table 1.** The voltages that needed to be applied to the four electrodes ( $V_A$ ,  $V_B$ ,  $V_C$ , and  $V_D$ ) in order to generate an electric field along nine different orientations in the plane of the device.

Electric field orientation (deg.) (relative to the $-y$ direction)	$V_A$ [V]	$V_B$ [V]	$V_C$ [V]	$V_D$ [V]
0	+70.71	+70.71	−70.71	−70.71
11.25	+55.55	+83.14	−55.55	−83.14
22.50	+38.26	+92.38	−38.26	−92.38
33.75	+19.51	+98.08	−19.51	−98.08
45	0	+100	0	−100
56.25	−19.51	+98.08	+19.51	−98.08
67.50	−38.26	+92.38	+38.26	−92.38
78.75	−55.55	+83.14	+55.55	−83.14
90	−70.71	+70.71	±70.71	−70.71

As an example, a combination of voltages was chosen such that the central region between the electrode areas switched ON by creating an electric field along  $+45^\circ$  with respect to the  $-y$ -axis. The magnitudes of the voltages were varied to estimate the threshold voltage required to switch the device. It was found that the LC director began to reorient at the electrode edges when a voltage of  $\pm 10$  V was applied, but that a reorientation of the LC director throughout the electrode gap did not occur until the applied voltage was between  $\pm 30$  V and  $\pm 40$  V (see Figure S3, Supporting Information). Furthermore, a defect line also appeared in the central region between the electrodes, which settled within a few minutes after the application of an electric field. This defect line appeared due to the asymmetric tilt of the LC director; that is, the LC director in the region left of the defect line tilted in one direction (say clockwise) when the electric field was applied whereas the LC director on the right side of the defect line tilted in the opposite direction and thereby a defect appeared where the two domains met. These defect lines are unwanted as they can affect the wavefront of the light passing through the device. Therefore, the voltages were adjusted so that the defect line would move towards the corner region of the active area.

To confirm that the device was capable of generating an electric field along different orientations in the plane of the device, the voltages that were estimated using Equations (1)–(6) to generate electric fields along a direction from  $0^\circ$  to  $180^\circ$  (relative to the  $-y$  direction) were applied to the four electrodes of the nematic LC device. To observe this behavior, the device was rotated in the plane and the corresponding voltage combination was then applied to obtain an electric field that was aligned with the polarizer so that a dark state was observed in the central region between the electrodes. An example of this can be seen in the polarized optical microscope images presented in Figure 3, which show that by adjusting the voltage combination to the electrodes, an electric field can be generated along different directions (relative to the  $+y$  direction) in the center of the active region. Images are shown for nine different orientations of the electric field in the plane of the device ranging from  $0^\circ$  to  $90^\circ$ . Table 1 summarizes the values of the voltages applied to the electrode in order to generate an electric field along preferentially the nine different orientations presented in Figure 3. Because of the variable anisotropy between the electrodes, and

the potential for defect formation, the voltages applied, as listed in Table 1, correspond to the different cases when the axis of ellipticity can be oriented in any direction at the center of the electrode structure away from the electrode edges and corners. The axis of ellipticity corresponds to the plane of the director, assuming that there is no twist.

## 2.2. Calibration of the Polarization Controller

To confirm that the device could be used to control and tune the polarization state of a polarized light source, and that it could generate a polarization state along any orientation through the application of a certain combination of voltages applied to the electrodes, the device was first tested with a continuous wave He-Ne laser (see the Experimental Section as well as Section S3, Supporting Information). Here a quarter waveplate designed for operation at  $\lambda = 632.8$  nm was used to convert the input linearly polarized light into circularly polarized light, which is relevant for the demonstration of the all-LC-based polarization controllable band-edge laser.

In the current setup a fixed combination of voltages was applied to the electrodes. For each combination of voltages, the polarization states were recorded via an A/D converter (National Instrument, USB-8451) and then numerically extracted. Since the nematic LC device can generate any polarization state with a particular orientation, to demonstrate this, a combination of voltages was chosen so as to generate an electric field at  $+45^\circ$  so as to give an orientation of the polarization at  $0^\circ$  and  $90^\circ$  and then the magnitude of the electric field was varied to change the retardance of the LC layer and hence change the polarization state from circular, to elliptical, to linear and so on.

Alternatively, to obtain an electric field that was aligned along  $0^\circ$ , the voltages at the electrodes were set as  $V_A = V_B = +V$ ,  $V_C = V_D = -V$ . Following this, the voltages were varied to change the retardance of the LC and thereby the corresponding polarization state (e.g., linear, circular, etc.). The results of the polarization states that were generated with the electric field along the  $+45^\circ$  orientation (with respect to the  $-y$ -direction) are presented in Figure 4. Each ellipse presented in the figure was generated by extracting and comparing the peak-to-peak voltage and phase values between the Signal and

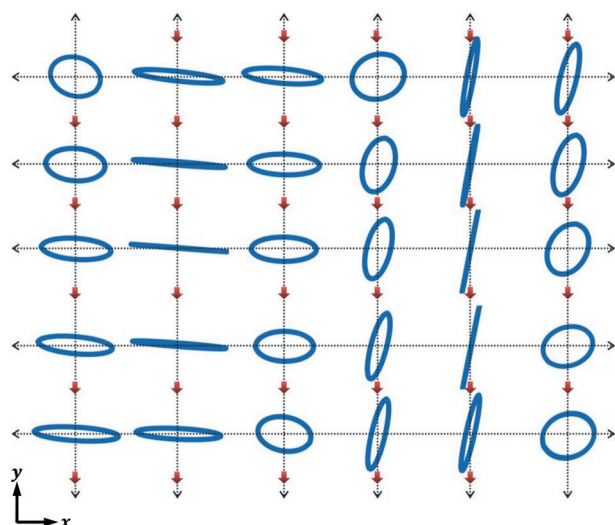


**Figure 4.** The polarization states of the He-Ne laser that were generated with the homeotropically aligned nematic LC device by applying the relevant combinations of voltages so as to create an electric field oriented along  $+45^\circ$  (relative to the  $-y$ -axis). In the figure, the horizontal and vertical axes represent the  $x$  and  $y$ -components of the light intensity in the polarization ellipses, respectively. To obtain these results, the voltage combination on each electrode was set as  $V_A = V_C = 0$  V,  $V_B = +V$ , and  $V_D = -V$ . The voltages  $V_B$  and  $V_D$  were then varied from  $\pm 100$  to  $\pm 67$  V (in general in step sizes of 1 V, see Table S1, Supporting Information) to achieve a complete set of polarization states as shown here. The red arrows indicate the sequence starting from the top left ( $\pm 100$  V) progressing from column to column down to the bottom right ( $\pm 67$  V) polarization state.

Reference beams. While the peak-to-peak voltage gives the ellipticity, the phase provides information about the orientation of the ellipse. Examples of the Signal and Reference beam waveforms for a number of different polarization states with their corresponding ellipses obtained from the experimental data are presented in Figure S5 of the Supporting Information.

It can be seen from Figure 4 that the polarization state starts from being circular (of one handedness) before changing to elliptical and then a linearly polarized state as the voltage amplitude is increased. While the different polarization states are achieved by changing the magnitude of the applied electric field along the  $+45^\circ$  direction, there appeared to be some deviation of the orientation of the generated polarization state. Theoretically, the electric field along the  $+45^\circ$  direction should result in linear polarization along either  $0^\circ$  or  $90^\circ$  (which is determined by the optical anisotropy offered by the LC at the given electric field amplitude, see Figure S6, Supporting Information). However, the experimentally generated (linear) states (as shown in Figure 4) deviated from theoretical predictions by  $\pm 3^\circ$ . This small discrepancy may be due to the nonuniform electric field distribution in the region where the laser passes through the device. For example, one possible reason for the discrepancy is that the nonuniform electric field could be the result of the nonsymmetrical shape of the fabricated indium tin oxide electrodes. Alternatively, the discrepancy may also be due to one or a combination of other factors such as the presence of defects in the nematic LC device, imperfect cell spacing and homeotropic alignment, as well as surface pinning of the LC director.

The next stage was to change the orientation of the electric field to demonstrate the manipulation of the orientation of the polarization state. Figure 5 presents results that demonstrate a few examples of circular, elliptical and linear polarization states on a Poincaré sphere as well as a “constellation of polarization states” (which can be considered as a 2D analogue of a Poincaré sphere). The orientation of the polarization states generated were at  $0^\circ$ ,  $22.5^\circ$ ,  $45^\circ$ ,  $67.5^\circ$ ,  $90^\circ$ ,  $-67.5^\circ$ ,  $-45^\circ$ , and  $-22.5^\circ$ . Examples of the orientation of the applied electric field and the resulting polarization states are shown in Figure S7 of the Supporting Information. Even though the electric field was applied to create the orientation of the polarization states at the chosen angles, the experimental results showed some level of deviation from the orientation at the said angles. As discussed previously, this may be due to imperfections in the symmetry of the four electrodes, slight deviations in the applied voltage from the waveform generator, the presence of defects in the nematic LC device, etc.

### 2.3. Tuning the Polarization of a Band-Edge LC Laser

To demonstrate control of the various polarization states of the LC band-edge laser when combined with the homeotropically aligned nematic LC device with the four-electrode configuration, the voltage levels were chosen as so to generate an electric field in the horizontal, vertical, and then diagonal directions in the active region between the electrodes. First, the voltage combination was set as  $V_A = V_B = +V$  and  $V_C = V_D = -V$ , which created an electric field in the vertical orientation (i.e.,  $0^\circ$  with respect to the  $-y$ -direction). Then the magnitude of the electric field was changed, which in turn varied the retardation of the nematic LC, thus resulting in changes to the polarization states of the LC laser from circular to elliptical and so on. Similarly, the voltage combination was altered so as to generate an electric field in the horizontal direction within the in-plane electrode region, and finally along the various diagonal orientations. For each combination of applied voltage, the minimum ( $V_{\min}$ ) and maximum ( $V_{\max}$ ) voltage levels recorded by the photodiode were read on the oscilloscope. These voltages defined the major and minor axes of the ellipse. By rotating the analyzer, the positions where these maximum and minimum voltages occurred provided the orientation of the corresponding major and minor axes for the ellipse (see the Experimental Section for further detail).

A constellation diagram showing the different polarization states is presented in Figure 6. It can be seen that the main polarization states created were as follows: circular of one handedness, elliptical, reverse elliptical and circular with opposite handedness oriented at  $0^\circ$ ,  $\pm 45^\circ$ , and  $90^\circ$ . As an example, polarization states created along the  $0^\circ$  or  $90^\circ$  directions are the result of a voltage combination that generates an electric field along the  $\psi = \pm 45^\circ$  orientations. For each orientation, the nematic LC device showed a range of polarization states from circular with one handedness to elliptical to circular with opposite handedness and so on. However, the device showed limitations in terms of the degree of linearity of the linear polarization state. This is considered to be due to the imperfect nature of the circular polarization of the band-edge LC laser which does not appear to be a well-defined polarization state—this



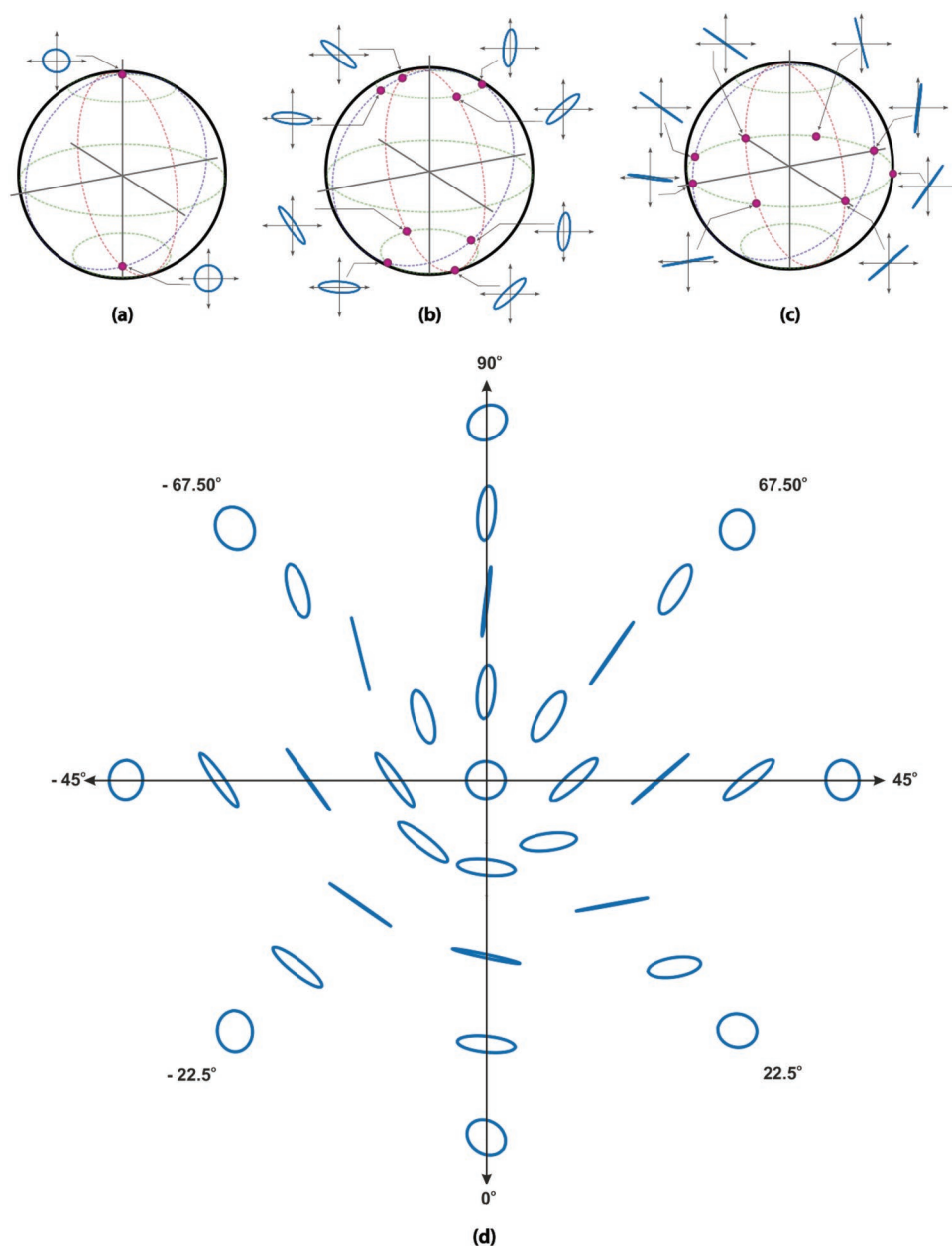


**Figure 5.** Poincaré sphere depicting examples of a) circular, b) elliptical, and c) linear polarization states of the He-Ne laser after passing through the homeotropically aligned nematic LC device with the four-electrode in-plane configuration. d) A complete set of polarization states with different orientations presented as a constellation diagram. The various polarization states were created by selecting the necessary relative combination of voltages to define the orientation of the polarization state whereas the magnitude of the applied electric field defines the actual polarization state (e.g., circular, linear, etc.).

may then limit the creation of linearly polarized light. Nevertheless, the device demonstrates a different polarization state along the other orientations such as  $+22.5^\circ$ ,  $+67.5^\circ$ ,  $-22.5^\circ$ , and  $-67.5^\circ$ . The exact voltage combinations applied to the electrodes are highly dependent on the device configuration (e.g., electrode gap, cell gap, LC dielectric/elastic/optical parameters), which have to be tuned to optimize polarization states and will vary from device-to-device.

By choosing a low repetition rate for the solid-state Nd:YAG pump laser to avoid photobleaching (see the Experimental

Section), the overall performance of the LC laser (in terms of excitation threshold and output power) remained stable. This was confirmed by monitoring the laser wavelength, output power, and polarization state throughout the measurement process. Before optically pumping the LC laser, the sample was inspected on a polarized optical microscope to identify regions where there was a uniform Grandjean texture corresponding to a single emission wavelength. This was also confirmed in reflection mode on the polarized optical microscope where a uniform single color was observed that corresponded to the central wavelength of the

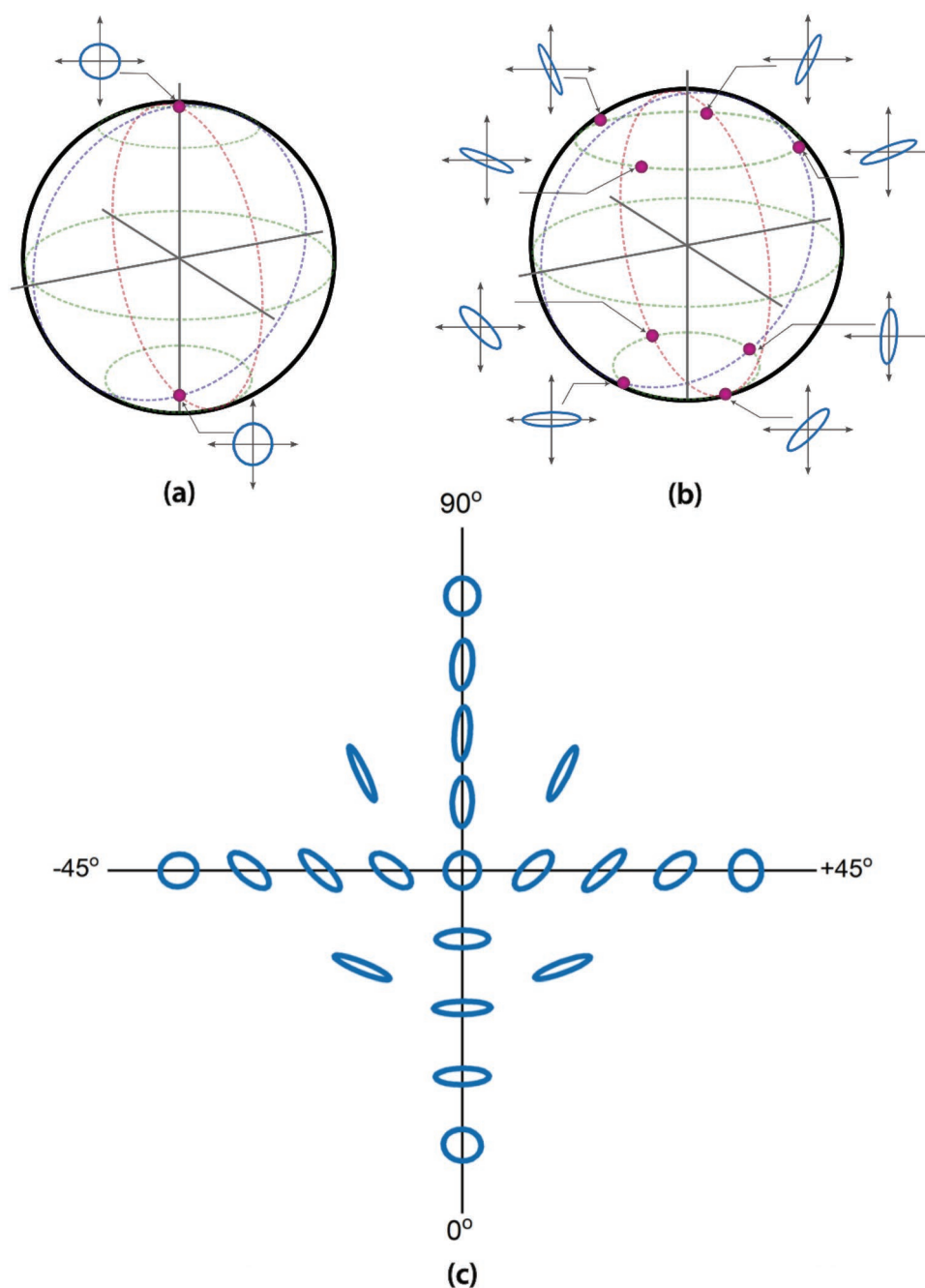


**Figure 6.** Poincaré spheres depicting examples of a) circular and b) elliptical polarization states of the band-edge LC laser after passing through the homeotropically aligned nematic LC device with the four-electrode in-plane configuration. c) A complete set of polarization states with different orientations presented as a constellation diagram. The various polarization states at different orientations were generated by applying different combinations of voltages and amplitudes to the nematic LC device.

reflection spectrum. Nevertheless, even if there had been some decrease in the output power of the LC laser in the longer term and provided that the optical pumping did not fall below the excitation threshold, then the changes in the intensity of the laser did not negatively impact the control of the polarization state. Techniques for maintaining the LC laser output at high pump repetition rates have been developed,<sup>[45]</sup> and the configuration presented here would be compatible with such strategies.

Previous reports that show polarization controllability using an LC device<sup>[26–34]</sup> do not typically control the orientation of the polarization state as well. Alternatively, the six-electrode-based device with SiO<sub>2</sub>–TiO<sub>2</sub> does enable control of orientation, but with an increase in the fabrication complexity.<sup>[35]</sup> The bench-top demonstration presented here suggests that a nematic LC device combined with a band-edge LC laser can be used to create any polarization state (e.g., linear, circular, etc.) along any



orientation by correctly choosing the appropriate voltage combination and amplitudes.

As both the laser and the polarization controller element are based upon liquid crystalline materials, this combination provides a direct route towards the integration of a band-edge laser with a nematic LC device to form an integrated polarization controllable LC laser. There are various strategies that could be adopted to develop a single integrated device comprising an LC laser and a tuneable nematic LC phase shifter. For example, a photopolymerized LC laser could be combined with a nematic LC with an electrode arrangement that is identical to the in-plane electrode configuration presented in the current study. In previous work, we have demonstrated how different polymerized layers can be integrated together to form more complex device architectures, such as a flexible defect mode laser<sup>[17]</sup> and a fast-switching phase modulator.<sup>[46]</sup> To develop the integrated device, the thickness of the in-plane electrodes would need to be controlled accurately and the refractive index matching between the chiral nematic and the nematic LC layer would require careful consideration to ensure that the internal reflection losses are minimized and to avoid any influence on the laser mode.

It is well known that the emission wavelength of an LC laser can be tuned using a variety of different external stimuli.<sup>[9–16]</sup> The addition of the polarization controller element could accommodate changes in the emission wavelength by adjusting the voltages applied to the electrodes. This would still maintain control of the polarization state, although a look-up table would be needed to establish the correct combination of voltages for each emission wavelength.

### 3. Conclusions

In summary, tuning of the polarization state (e.g., linear, circular or elliptical) and the orientation of the polarization (e.g., along the horizontal, vertical, diagonal axes relative to the plane of the device) of a band-edge LC laser has been demonstrated with the addition of a homeotropically aligned nematic LC device. Simulations carried out using finite element modeling, and assuming an isotropic dielectric permittivity, enabled the orientation of the electric field to be determined based upon the combination of voltages applied to the four in-plane electrodes. This combination of voltages was critical in terms of determining the orientation of the resulting polarization state of the laser. The bench top demonstration developed in this study shows that, in principle, the circularly polarized light that is emitted from a band-edge LC laser can be tuned to any polarization state with any desired orientation by correctly choosing the polarity and the magnitude of the applied electric field in the nematic LC device. Control of the polarization state of a band-edge LC laser is of particular interest in 3D, augmented reality, virtual reality, and holographic displays. Such a system could also be employed to create a compact all-in-one polarization-controllable thin-film laser for 3D imaging, which would be of significant importance for biomedical and future display systems. In future work, we hope to demonstrate the benefits of this full polarization control in a microscope imaging system

so that a range of images can be acquired for different polarization states that are readily accessible by just changing the applied voltage to the nematic LC layer. This approach would negate the need for multiple  $\frac{1}{4}$  or  $\frac{1}{2}$  waveplates that would have to be controlled mechanically. We also hope to test these polarization controllable lasers in an optical communications setting, so as to demonstrate polarization shift keying, for example.

### 4. Experimental Section

A chiral nematic LC band-edge laser was prepared using the laser dye, Pyrromethene 597 (PM597, Exciton). The PM597 laser dye was chosen because it is known to be soluble in liquid crystalline materials and has been shown to exhibit a high quantum efficiency when dispersed into an LC host.<sup>[47]</sup> Band-edge lasers fabricated using this laser dye have been found to exhibit relatively low excitation thresholds and high slope efficiencies.<sup>[47]</sup> The chiral nematic LC was prepared by doping the well-characterized nematic LC mixture, E7 (Synthon Chemicals Ltd.) with 3 wt% of the chiral dopant R5011 (Merck KGaA). The concentration of chiral dopant was chosen so that the long-wavelength edge of the photonic bandgap roughly coincided with the wavelength range corresponding to the emission peak of the laser dye ( $\lambda \approx 560\text{--}585\text{ nm}$ ). The sample was then capillary filled into a glass cell that consisted of antiparallel rubbed polyimide alignment layers. In this case, the LC layer thickness was  $5\text{ }\mu\text{m}$ . Inspection on a polarized optical microscope revealed that the average monodomain area was about  $400\text{ }\mu\text{m}^2$  in size, which was greater than the size of the illumination spot of the solid-state Nd:YAG laser that was used to optically pump the LC band-edge laser ( $325\text{ }\mu\text{m}^2$ ) (see also Section S4, Supporting Information, for further detail regarding the characterization of the LC laser).

The process for fabricating the nematic LC device and the experimental system used to measure the different polarization states of the band-edge LC laser is presented in Section S5 of the Supporting Information. To take the measurements of the polarization state, a manual method was adopted that consisted of rotating the analyzer from  $0^\circ$  to  $90^\circ$  while recording the photodiode output voltage on the oscilloscope. Depending on the applied voltage on the homeotropically aligned nematic LC device, the photodiode response showed a maximum ( $V_{\text{max}}$ ) or a minimum ( $V_{\text{min}}$ ) level as the analyzer was oriented through  $0^\circ$  to  $90^\circ$ . For example, if the applied voltage combination on the nematic device created linearly polarized light, rotating the analyzer from  $0^\circ$  to  $90^\circ$  appeared as a modulated signal with voltage changing from  $V_{\text{max}}$  to  $V_{\text{min}}$  ( $= 0\text{ V}$ ), respectively. However, for circularly polarized light, the corresponding modulation was zero and thus  $V_{\text{max}} = V_{\text{min}}$  as the analyzer is rotated from  $0^\circ$  to  $90^\circ$ .

For each applied electric field to the nematic LC device, the photodiode voltage level ( $V_{\text{max}}$  and  $V_{\text{min}}$ ) was recorded. As any polarization state can be represented as an ellipse, the dimensions of the major and minor axes varied depending upon whether the state was circular, elliptical or linear. The  $V_{\text{max}}$  and  $V_{\text{min}}$  levels, therefore, define the major and minor axes of the ellipse. While rotating the analyzer, the positions where  $V_{\text{max}}$  and  $V_{\text{min}}$  occurred were also recorded as they provided the orientation of the corresponding major and minor axes for the ellipse, and they were termed as  $\alpha_{\text{max}}$  and  $\alpha_{\text{min}}$ , respectively.

As the orientation of the analyzer was set either to  $\alpha_{\text{max}}$  or  $\alpha_{\text{min}}$ , which gives the corresponding photodiode signals,  $V_{\text{max}}$  or  $V_{\text{min}}$ , respectively, the change or gradient of the photodiode signal at these orientations was almost zero. This means that varying the orientation of the analyzer through a small angle around either  $\alpha_{\text{max}}$  or  $\alpha_{\text{min}}$  would not sufficiently vary the corresponding photodiode signal used to record the exact value of  $V_{\text{max}}$  or  $V_{\text{min}}$ . Therefore, after recording approximate values for  $V_{\text{max}}$  and  $V_{\text{min}}$  from the photodiode signal, the analyzer was then oriented half-way between  $V_{\text{max}}$  and  $V_{\text{min}}$  to record an average value

$V_{\text{avg}}$ ; the corresponding orientation of the analyzer was then  $\alpha_{\text{avg}} \approx 45^\circ$ . At this orientation of  $\alpha_{\text{avg}}$ , the analyzer was then oriented to  $+45^\circ$  and then  $-45^\circ$  and the corresponding new values for  $V_{\text{max}}$  and  $V_{\text{min}}$  were recorded, respectively. This ensured that the correct degree of ellipticity was recorded.

## Supporting Information

Supporting Information is available from the Wiley Online Library or from the author.

## Acknowledgements

T.A. thanks the Punjab Educational Endowment Fund (PEEF), Pakistan, and the Vicky Noon Education foundation for financial support during his graduate studies. The authors also gratefully acknowledge the Engineering and Physical Sciences Research Council (UK) for financial support through Project No. EP/R511742/1.

## Conflict of Interest

The authors declare no conflict of interest.

## Data Availability Statement

The data that support the findings of this study are available from the corresponding author upon reasonable request.

## Keywords

band-edge laser, chiral nematic liquid crystal, nematic liquid crystals, polarization controller

Received: April 23, 2022

Revised: July 31, 2022

Published online: November 6, 2022

- [1] J. Mysliwiec, A. Szukalska, A. Szukalski, L. Sznitko, *Nanophotonics* **2021**, *10*, 2309.
- [2] H. Coles, S. Morris, *Nat. Photonics* **2010**, *4*, 676.
- [3] V. I. Kopp, B. Fan, H. K. M. Vithana, A. Z. Genack, *Opt. Lett.* **1998**, *23*, 1707.
- [4] B. Taheri, A. Munoz, P. Palffy-Muhoray, R. Twieg, *Mol. Cryst. Liq. Cryst.* **2001**, *358*, 73.
- [5] Y. Watanabe, M. Uchimura, F. Araoka, G. Konishi, J. Watanabe, H. Takezoe, *Appl. Phys. Express* **2009**, *2*, 102501.
- [6] Y. Inoue, H. Yoshida, K. Inoue, A. Fujii, M. Ozaki, *Appl. Phys. Express* **2010**, *3*, 102702.
- [7] M. Uchimura, Y. Watanabe, F. Araoka, J. Watanabe, H. Takezoe, G. I. Konishi, *Adv. Mater.* **2010**, *22*, 4473.
- [8] C. Mowatt, S. M. Morris, T. D. Wilkinson, H. J. Coles, *Appl. Phys. Lett.* **2010**, *97*, 251109.
- [9] H. Finkelmann, S. T. Kim, A. Muñoz, P. Palffy-Muhoray, B. Taheri, *Adv. Mater.* **2001**, *13*, 1069.
- [10] M. Ozaki, M. Kasano, D. Ganzke, W. Hasse, K. Yoshino, *Adv. Mater.* **2002**, *14*, 306.
- [11] A. Chanishvili, G. Chilaya, G. Petriashvili, R. Barberi, R. Bartolino, G. Cipparrone, A. Mazzulla, L. Oriol, *Appl. Phys. Lett.* **2003**, *83*, 5353.
- [12] T. H. Lin, H. C. Jau, C. H. Chen, Y. J. Chen, T. H. Wei, C. W. Chen, A. Y. G. Fuh, *Appl. Phys. Lett.* **2006**, *88*, 061122.
- [13] Y. Huang, L.-P. Chen, C. Doyle, Y. Zhou, S.-T. Wu, *Appl. Phys. Lett.* **2006**, *89*, 111106.
- [14] Y. Huang, Y. Zhou, S.-T. Wu, *Appl. Phys. Lett.* **2006**, *88*, 011107.
- [15] S. Y. Cho, H. Yoshida, M. Ozaki, *Adv. Opt. Mater.* **2020**, *8*, 2000375.
- [16] S. Wood, F. Castles, S. J. Elston, S. M. Morris, *RSC Adv.* **2016**, *6*, 31919.
- [17] T. Ali, J.-D. Lin, B. Snow, X. Wang, S. J. Elston, S. M. Morris, *Adv. Opt. Mater.* **2020**, *8*, 1901891.
- [18] T. Matsui, R. Ozaki, K. Funamoto, M. Ozaki, K. Yoshino, *Appl. Phys. Lett.* **2002**, *81*, 3741.
- [19] C. M. Brown, D. K. E. Dickinson, P. J. W. Hands, *Opt. Laser Technol.* **2021**, *140*, 107080.
- [20] H. K. Shin, J. H. Lee, J.-W. Kim, T.-H. Yoon, J. C. Kim, *Appl. Phys. Lett.* **2011**, *98*, 063505.
- [21] B. M. A. Rahman, S. S. A. Obayya, N. Somasiri, in *Physics and Simulation of Optoelectronic Devices*, Vol. 4986, SPIE **2003**, pp. 363–374, <https://doi.org/10.1117/12.474374>.
- [22] G. D. VanWiggeren, R. Roy, *Appl. Opt.* **1999**, *38*, 3888.
- [23] D. Clarke, J. Grainger, in *Polarized Light and Optical Measurement* (Eds: D. Clarke, J. Grainger), Pergamon, Oxford **1971**, p. 155.
- [24] I. Kaminow, *IEEE J. Quantum Electron.* **1981**, *17*, 15.
- [25] D. L. Hickman, M. I. Smith, K. S. Kim, H.-J. Choi, in *In Electro-Optical and Infrared Systems: Technology and Applications XV*, Vol. 10795, **2018**, SPIE, pp. 79–98, <https://doi.org/10.1117/12.2325320>.
- [26] F. Cheng, L. Ding, L. Qiu, D. Nikolov, A. Bauer, J. P. Rolland, A. N. Vamivakas, *Opt. Express* **2018**, *26*, 30678.
- [27] K. Iizuka, in *Three-Dimensional and Multidimensional Microscopy: Image Acquisition and Processing XV*, Vol. 6861, SPIE, **2008**, pp. 227–237, <https://doi.org/10.1117/12.760085>.
- [28] H. Chen, Y. Weng, D. Xu, N. V. Tabiryan, S.-T. Wu, *Opt. Express* **2016**, *24*, 7287.
- [29] Z. S. Hou, X. Xiong, J. J. Cao, Q. D. Chen, Z. N. Tian, X. F. Ren, H. B. Sun, *Adv. Opt. Mater.* **2019**, *7*, 1900129.
- [30] H. Ren, S.-T. Wu, *Appl. Phys. Lett.* **2007**, *90*, 121123.
- [31] F. Yang, L. Ruan, S. A. Jewell, J. R. Sambles, *Opt. Express* **2007**, *15*, 4192.
- [32] Z. Zhuang, S.-W. Suh, J. Patel, *Opt. Lett.* **1999**, *24*, 694.
- [33] C. Ye, *Opt. Eng.* **1995**, *34*, 3031.
- [34] J. A. Davis, D. E. McNamara, D. M. Cottrell, T. Sonehara, *Appl. Opt.* **2000**, *39*, 1549.
- [35] L. M. Chang, C. C. Yin, C. Y. Lin, C. T. Wang, Y. J. Hung, *Liq. Cryst.* **2020**, *48*, 806.
- [36] A. Gevorgyan, M. Harutyunyan, K. Oganessian, M. Rafayelyan, *Optik* **2012**, *123*, 2076.
- [37] A. Gevorgyan, K. Oganessian, *J. Contemp. Phys. (Arm. Acad. Sci.)* **2010**, *45*, 209.
- [38] C.-J. Yu, C.-M. Hsieh, *IEEE Photonics Technol. Lett.* **2016**, *28*, 1229.
- [39] M. Honma, K. Okitsu, T. Nose, *Jpn. J. Appl. Phys.* **2013**, *52*, 022501.
- [40] T.-Y. Chung, M.-C. Tsai, C.-K. Liu, J.-H. Li, K.-T. Cheng, *Sci. Rep.* **2018**, *8*, 13691.
- [41] N. Kundikova, I. Popkov, A. Popkova, *Appl. Opt.* **2010**, *49*, 6504.
- [42] A. Safrani, I. Abdulhalim, *Opt. Lett.* **2009**, *34*, 1801.
- [43] C.-T. Wang, T.-H. Lin, *J. Appl. Phys.* **2010**, *107*, 123102.
- [44] R. Ozaki, M. Ozaki, K. Yoshino, *Crystals* **2015**, *5*, 394.
- [45] M. C. Normand, P. Chen, C. Can, P. J. W. Hands, *Opt. Exp.* **2018**, *26*, 26544.
- [46] X. Wang, J. A. Fells, Y. Shi, T. Ali, C. Welch, G. H. Mehl, T. D. Wilkinson, M. J. Booth, S. M. Morris, S. J. Elston, *Adv. Mater. Technol.* **2020**, *5*, 2000589.
- [47] C. Mowatt, S. M. Morris, M. H. Song, T. D. Wilkinson, R. H. Friend, H. J. Coles, *J. Appl. Phys.* **2010**, *107*, 043101.